Progress In Electromagnetics Research B, Vol. 24, 173–189, 2010

A COMPACT QUAD-BAND PIFA BY TUNING THE DEFECTED GROUND STRUCTURE FOR MOBILE PHONES

D.-B. Lin

Department of Electronic Engineering
National Taipei University of Technology
1, Sec. 3, Chung-Hsiao E. Rd., Taipei 10608, Taiwan, R.O.C.

I-T. Tang

Department of Greenergy
National University of Tainan
33, Sec. 2, Shu-Lin St., Tainan 70005, Taiwan, R.O.C.

M.-Z. Hong

Department of Electronic Engineering
National Taipei University of Technology
1, Sec. 3, Chung-Hsiao E. Rd., Taipei 10608, Taiwan, R.O.C.

Abstract—The development of compact antennas plays an important role in the rapidly growing mobile communication market. This paper presents a novel design technique of the quad-band small internal antenna covering GSM-900/DCS-1800/PCS-1900/IMT-2000 bands. The innovative quad-band built-in handset antenna is developed within the limit of a $44\times25\times4\,\mathrm{mm}^3$ volume. The following document describes a new idea of increasing operational bandwidth for the compact planar inverted F antenna (PIFA). The proposed compact antenna introduces the open-end slots in the ground plane almost all under the radiating patch. The size reduction method is attractive for practical antenna implementations. In addition, the end user's hand handling effects on the performances of the proposed antenna are studied.

Received 6 July 2010, Accepted 7 August 2010, Scheduled 13 August 2010
Corresponding author: I-T. Tang (tangitseng@gmail.com).

1. INTRODUCTION

As mobile communications grow rapidly, it is desirable for a single handset to access the additional several services such as voice, data, and video at anytime and anywhere. Devices capable of operating at multiple frequency bands, specifically within the quad-band standard, as a result, has seen increases in demand. At the same time, the wireless handset adapts the internal antenna structure also, due to popularities. Therefore, small size and multi-band internal antennas for wireless terminal has been an increasingly important issue.

The planar inverted-F antenna (PIFA) has a desirable multi-band feature with higher efficiency, low profile and lightweight internal antenna. This structure can be easily incorporated into personal communication equipment, reported in [1–7]. Due to these advantages, PIFA become attractive candidates in wireless communications. But the narrow bandwidth characteristic of PIFA is one of the limitations for its commercial application for wireless mobile terminals. With the extension of PIFA type structure, the novel broadband internal antenna which operates at the GSM (880–960 MHz)/DCS (1710–1880 MHz)/PCS (1850–1990 MHz)/IMT-2000 (1920–2170 MHz) quad-band is introduced in this paper.

For mobile phones, the main objectives which are necessary for investigations include the properties of antenna elements, bandwidth enhancement, efficiency and size [8, 9]. It has also been well known that the performance, especially the bandwidth enhancement, is largely defined by the combined behavior of the antenna and the phone chassis. In many published small-antenna designs the antenna is mounted on a phone chassis, and from the large bandwidths obtained it can be assumed that the effect of the chassis is significant [10, 11], however, the effect of the chassis is usually not analyzed. For fairly large portable radios, the effect of the dimensions of the chassis on the bandwidth was studied in [12]. Recently, this effect has been investigated for smaller devices with chassis or circuit-board length in the range of 80–150 mm, typical to current mobile phones [13]. It was noticed that the bandwidth for 900 MHz patch antennas had very clear dependency on the length of the chassis. For some antenna types the maximum bandwidth was over five-times larger than the minimum, and the maximum bandwidth was obtained with chassis length of about 130 mm. These results indicate that the total radiation bandwidth of the antenna-chassis combination is largely defined by the dipole-type radiation of the chassis currents, whose level further depends on whether the chassis is at resonance or not. Therefore, it is necessary to utilize the whole metallic structure of the handset to obtain the

required bandwidth, and there is also an obvious connection between the bandwidth, and radiation patterns of mobile-phone antennas.

The utilization of a slotted ground plane for broadening operational bandwidth of a small terminal antenna was described in [14–16]. These authors developed circuit models explaining interactions between a primary radiating element, such as a planar inverted F antenna (PIFA), and a finite ground plane/chassis. Using these models they showed that the size and shape of chassis could play a significant role in broadening operational bandwidth of a terminal antenna. In particular, they pointed out that slots in a chassis could assist optimizing the antenna operational bandwidth.

A new solution to broadening operational bandwidth of a compact quad-band planar inverted F-type antenna is proposed. This new idea will present the significance of the chassis effect with a rather simple but adequately accurate equivalent circuit model based on an approximate modal analysis of the fields and waves on the handset structure. In addition, the user's hand's impact on the performance of a PDA phone with the proposed antenna is considered and analyzed.

2. SYSTEM DESCRIPTIONS

2.1. The Wavemodes of the Antenna-chassis of Quad-band PIFA Combination

The maximum dimension (lengthwise) of current mobile handsets is less than half a wavelength at 900 MHz. The other dimensions including those of the antenna elements are clearly smaller. Thus, the structure can support only a few significant wavemodes. In this paper, we divide the structure into two significant parts: the antenna element (primary radiating element) and the chassis. In the antenna element of current, mobile handsets is usually self-resonant and has some characteristic wavemodes, which is typically a slow-wave mode like in normal mode helices or a reactively loaded quasi-TEM mode like in PIFA (or patch antennas). The fields and currents of this wavemode are concentrated in the vicinity of the small antenna element and for this mode the chassis acts as a ground plane with confined currents creating the mirror-image effect for the antenna element. The length of the handset chassis or circuit board is clearly larger than the width or the thickness, and therefore the structure also supports single-wire or thick-dipole type current distributions. Here, the fields and currents are distributed over the whole structure and thus, the distribution is clearly less concentrated spatially than the antenna-element wavemode.

Due to the small electrical size of the antenna and the chassis, the frequency response of the wavemodes is characterized by lowest

order resonances including one to three standing wave "lobes". The basic idea presented here is that while considering its radiation and circuit properties, the antenna-chassis combination can be described by combining the separate radiations and impedance characteristics of the wavemodes of the antenna element and the phone chassis. These characteristics are defined by the respective current distributions and resonant responses. Furthermore, as is well-known, the impedance and the surface field distribution of an antenna are connected through a surface integral relationship [17]. Thus, it is also possible to study the relationships between impedance properties and radiated fields, especially when it comes to resistive components of the impedance and the radiated power. The contributions from each part of the combination to radiated power, near fields, and bandwidth are largely defined by the relative amplitudes of the wavemodes, which can be selected by tuning the coupling between the wavemodes. Accurate determination of the radiation properties of the antenna-handset combination requires, of course, a complete analysis of the combined wave distribution with, for instance, numerical methods; but the modal analysis presented here can be used to identify main aspects of the radiation, especially in the cases where either one of the wavemodes dominates clearly. The impedance bandwidth is also defined by the coupling and the impedance match of the antennas.

2.2. The Similarly Equivalent Circuit of Quad-band PIFA

When investigating a small antenna element located in a phone chassis, it can be noticed that, the currents flowing on the chassis are induced through electromagnetic coupling from the antenna element, which is further excited by its feed. As the antenna is self-resonant and the length of the chassis is often close to some multiples of half wavelength, the obvious lumped-component combined equivalent circuit model of the proposed quad-band PIFA can be shown in Fig. 1. The resonant mode can be modeled an equivalent circuit which parallel component resister, capacitor and inductance. Resonators 1 and 4 represent the antenna element (primary radiating element), while resonators 2 and 3 represent the phone chassis (ground element). When resonator 1 (920 MHz) is excited. The current is more distributed on L1, C1 and G1 as Fig. 4(a). Resonator 2, 3 (1750 MHz, 2030 MHz) is excited. Current is often located on components L2 (L3), C2 (C3) and G2 (G3) as behavior of electric fields distributed on slot as Figs. 5 (Fig. 6). L-PIFA could model like circuit L4, C4 and G4. Thus resonator 4 (2200 MHz) is excited. The current will distribute on L-PIFA as Fig. 4(b). However, it is known that the impedance behavior of a shorted probe-fed PIFA is close to that of a parallel resonant circuit.

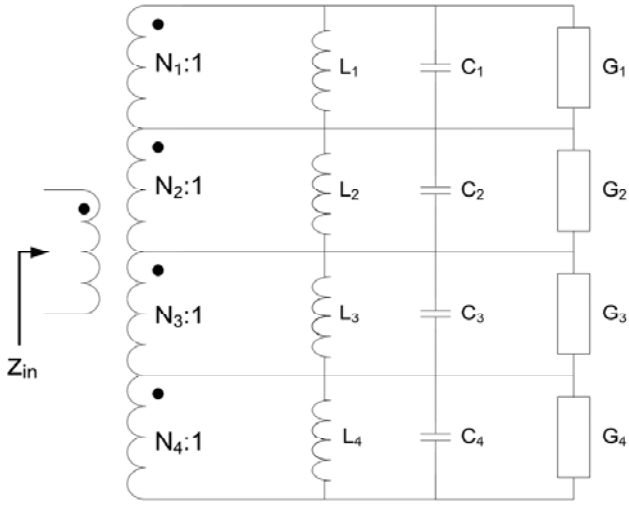

Figure 1. Equivalent circuit model of the proposed quad-band PIFA.

The inductance of the probe can be included in the model but they are not significant from the main results. Furthermore, every resonator can also be considered to be a nonradiating matching circuit, providing only coupling to the radiating resonator.

The input impedance Z_{in} of the equivalent circuit model in Fig. 1 for each resonant frequency can be given by (1)

$$Z_{in} = \frac{N_x^2}{\frac{1}{j\omega L_x} + j\omega C_x + G_x} \quad x = 1 \sim 4 \tag{1}$$

3. ANTENNA ANALYSIS AND DESIGN

3.1. Antenna Structure

The considered antenna configuration (top and side view) is shown in Fig. 2. The commercial program high frequency structure simulator (HFSS) based on the finite-element method (FEM) is used for analyzing the behavior of proposed model and determining suitable values of parameters. As seen in this figure, the antenna comprises a meander radiating path and L-shape radiating path of primary radiating element with a low-cost FR4 substrate with dielectric constant $\varepsilon_r = 4.4$, loss tangent $\tan\delta = 0.02$, and thickness $h = 0.4\,\text{mm}$ in the first layer, a defect ground plane with a FR4 substrate in the second layer, a short-circuited strip, and a coaxial probe. The primary

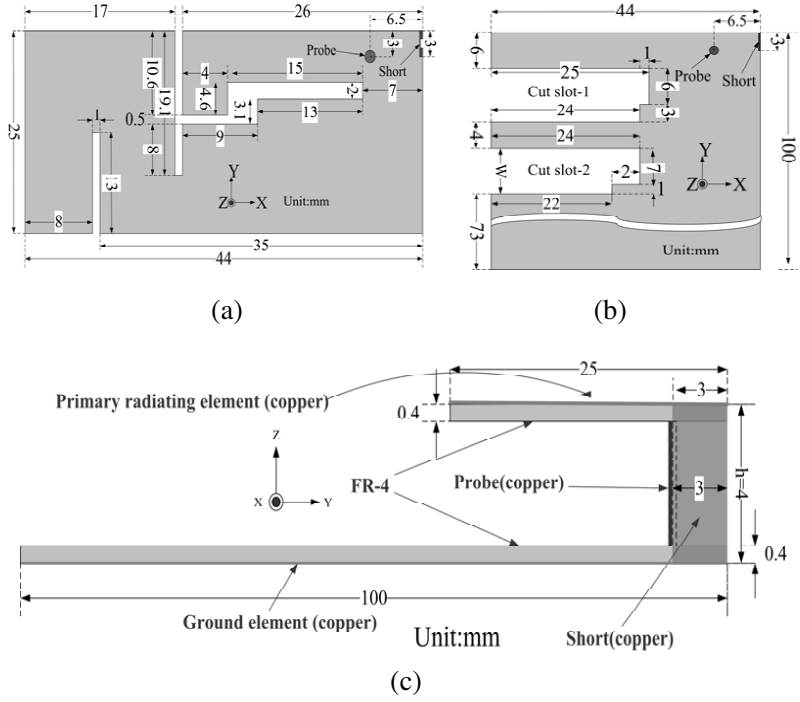

Figure 2. Geometry and dimensions (a) primary radiating element, (b) defected ground plane, and (c) complete antenna structure (side view).

radiating element is connected to the ground plane by a vertical short-circuited strip and is fed via a coaxial probe feed connected to a transmission line, which in the present case is assumed to have a characteristic impedance of 50 Ω. The quad-band planar inverted F antenna (PIFA) is spaced from the ground plane by a dielectric substrate of air. At the first layer, the long meander path portion of primary radiating element of the antenna is tuned to have a relatively lower band resonance frequency, such as first mode (900 MHz), and the short L-shape path part of primary radiating element of the antenna is tuned to have a higher band resonance frequency, such as fourth mode (2.2 GHz). The resonant frequencies of the antenna can be approximately determined by (2) [18, 19]

$$(L + W) = \frac{\lambda}{4(\sqrt{\varepsilon_r})} \tag{2}$$

where λ is resonance wave length at band, L and W are length and width of the radiating surface at operating band, ε_r is dielectric constant of the substrate.

At the second layer, the cut slot-1 and cut slot-2 of incoherent slot portion of ground element of the antenna is tuned to have a relatively higher band resonance frequency, such as second mode (1.75 GHz) and third mode (2.03 GHz). The handset antenna is developed within the limits of a $44 \times 25 \times 4$ mm^3. The ground plane element has dimensions of length 100 mm, and width 44 mm. The dimensions of the quad-band planar inverted F antenna (PIFA) are shown in Fig. 2.

Figure 3(a) shows the geometry of the antenna enclosed by the housing of the mobile phone, and the side view of the geometry is shown in Fig. 3(b). The mobile phone housing is fabricated using a 1-mm thick acrylonitrile butadiene styrene (ABS) plate with relative permittivity (ε_r) 3.5 and conductivity (σ) 0.02 S/m. The ABS is a practical material for housing general mobile phones. The housing can avoid direct contact of the user's hand with the antenna and the system ground plane in the experiment.

3.2. Current Distribution of 0.92 GHz and 2.2 GHz

In order to check the current flows at the resonance frequencies, the simulated results of the excited patch surface currents at 0.92 GHz and 2.2 GHz are presented in Fig. 4. At the resonance frequency of 0.92 GHz

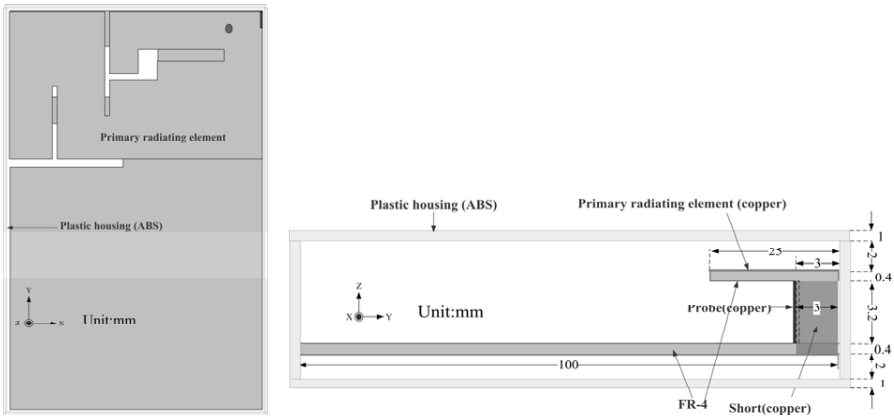

(a) (b)

Figure 3. (a) Geometry of the proposed antenna enclosed by the housing of the mobile phone, (b) side view.

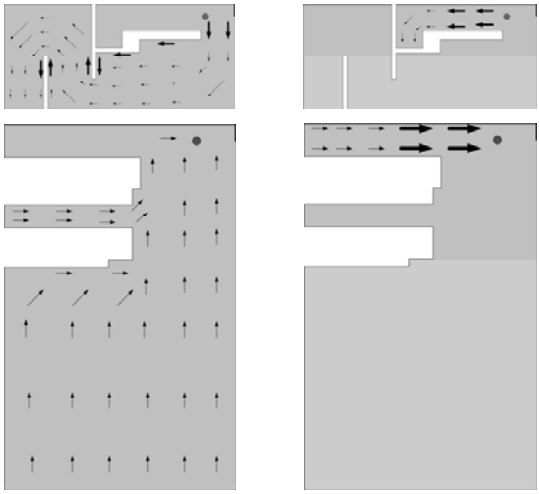

Figure 4. Simulated patch surface current distributions of the proposed antenna (a) 0.92 GHz, (b) 2.2 GHz.

in Fig. 4(a), the upper current paths starting from short-circuited strip post are passing through the meander path. These total length of the current paths are about 85 mm, an approximately quarter-wavelength at the GSM band. Fig. 4(a) shows the current distribution of ground element at 0.92 GHz.

At the resonance frequency of 2.2 GHz in Fig. 4(b), the lower current paths starting from short-circuited strip post are passing through the L-shape path. These total lengths of the current paths are about 36 mm, or approximately quarter-wavelength at the IMT-2000 band. Fig. 4(b) shows the current distribution of ground element at 2.2 GHz.

3.3. Field Distribution of 1.75 GHz and 2.03 GHz

The electric field distributions of these resonant modes are simulated investigated at second resonant mode 1.75 GHz and third resonant mode 2.03 GHz, as shown in Figs. 5 and 6, respectively.

Figure 5 shows the second resonant mode at 1.75 GHz where both x- and y-component fields exist in cut slot-1 and cut slot-2. Note that the x-component fields of the left and right sides of the slots are becoming periodicity from right to left. Therefore the electric fields radiates from cut slot-1 and cut slot-2 to far fields. The y-component

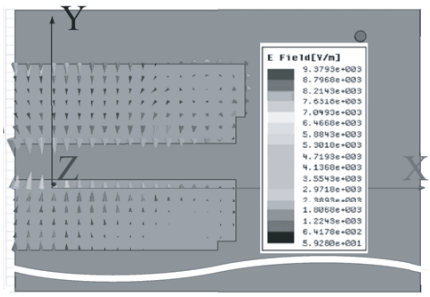

Figure 5. Electric fields distribution of second resonant mode at 1.75 GHz.

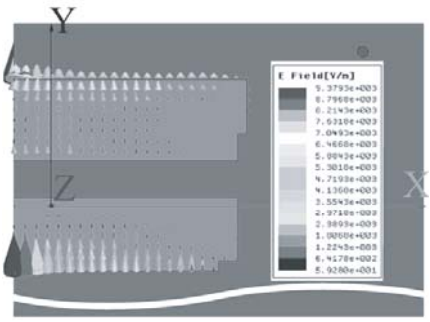

Figure 6. Electric fields distribution of third resonant mode at 2.03 GHz.

fields of cut slot-1 and cut slot-2 are in the opposite directions that influence each other at far fields in the asymmetric E-plane.

Figure 6 shows the third resonant mode at 2.03 GHz where both x- and y-component fields exist in cut slot-1 and cut slot-2. Note that the x-component fields of the left and right sides of the slots are becoming periodicity from right to left. Therefore the electric fields radiates from cut slot-1 and cut slot-2 to far fields. The y-component fields of cut slot-1 and cut slot-2 are in the same directions that influence each other at far fields in the asymmetric E-plane.

3.4. Parametric Study

In this section, effects of varying key antenna parameters, i.e., the size of cut slot-1 of ground element, the size of cut slot-2 of ground element, and comparisons of defect ground structure (DGS) and ordinate ground plane are considered on the antenna bandwidth. For reflection coefficient characteristic (S_{11}) less than -7.5 dB (VSWR $\leq$ 2.5), as observed in Fig. 7 with either the ordinary or slotted ground plane is used respectively to compare their resonant frequencies, operational bandwidth and impedance characteristics. It shows that, two parallel open-end slots in the ground plane, almost under the primary radiating element, were successfully used for broadening the antenna bandwidth.

The first variation is performed by varying the size of cut slot-1 of ground element, as shown in Fig. 8(a). Other parameters of primary radiating element of the antenna are presented in Fig. 2(a). It can be seen from Fig. 9, that this variation has a large impact creating new wavemodes of the higher frequency band.

The second variation is performed by varying the size of cut slot-2

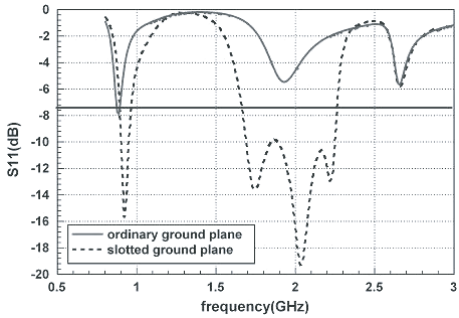

Figure 7. Simulated reflection coefficients S_{11} with either ordinary or slotted ground plane respectively.

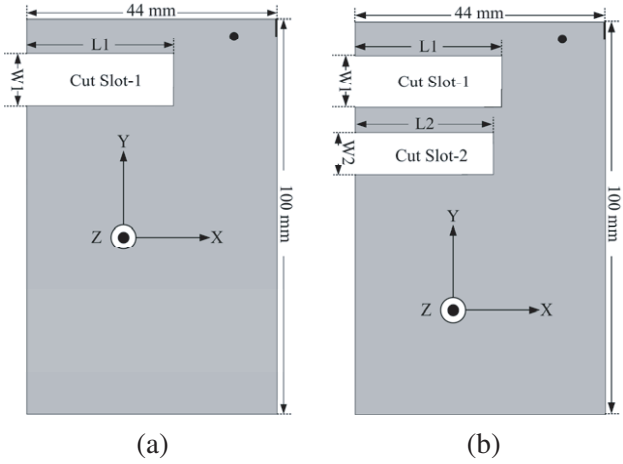

Figure 8. Geometry and configuration (a) only cut slot-1 of defect ground structure of proposed antenna, (b) both cut slot-1 and cut slot-2 of defect ground structure of proposed antenna.

of ground element, as shown in Fig. 8(b). Other parameters of primary radiating element of the antenna are presented in Fig. 2(a). It can be seen from Fig. 10, that this variation has a large impact on the impedance matching of the higher frequency band.

While the results shown in Fig. 11 indicate that the two cut slots, responsible for enhancing the antenna performance in the higher frequency band, are optimally designed by turning both slots geometry to the specification shown in Fig. 2(b).

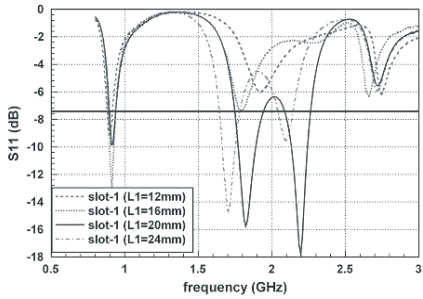

Figure 9. Simulated S_{11} and reflection coefficients with slotted ground plane by different length with fix width of cut slot-1 of ground element.

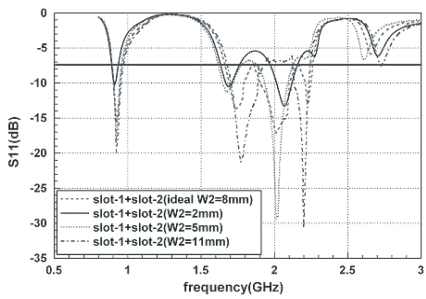

Figure 10. Simulated S_{11} and reflection coefficients with slotted ground plane by different width with fix length of cut slot-2 of ground element.

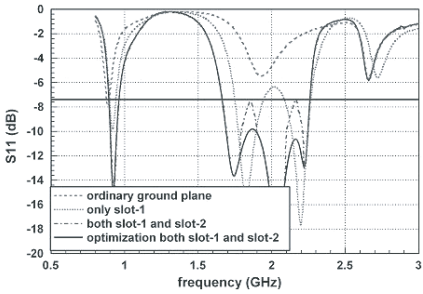

Figure 11. Simulated S_{11} with slotted ground plane by compare to different slotted of defect ground structure (DGS).

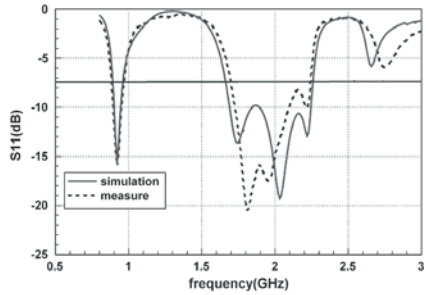

Figure 12. Simulated and measured results of S_{11} of the proposed antenna.

4. RESULTS AND DISCUSSIONS

4.1. Impedance Bandwidth

The measurement of return loss is carried out with an HP8720C network analyzer. The radiation patterns are measured in a far-field anechoic chamber. Fig. 12 shows the simulated and measured reflection coefficient (S_{11}), from which we can see that the simulated and measured results agree with each other. The input impedance is well matched as the reflection coefficient (S_{11}) less than -7.5 dB (VSWR $<$ 2.5). The entire achieved bandwidth is 882–965 MHz for the GSM band and 1702–2235 MHz for the higher bands, which

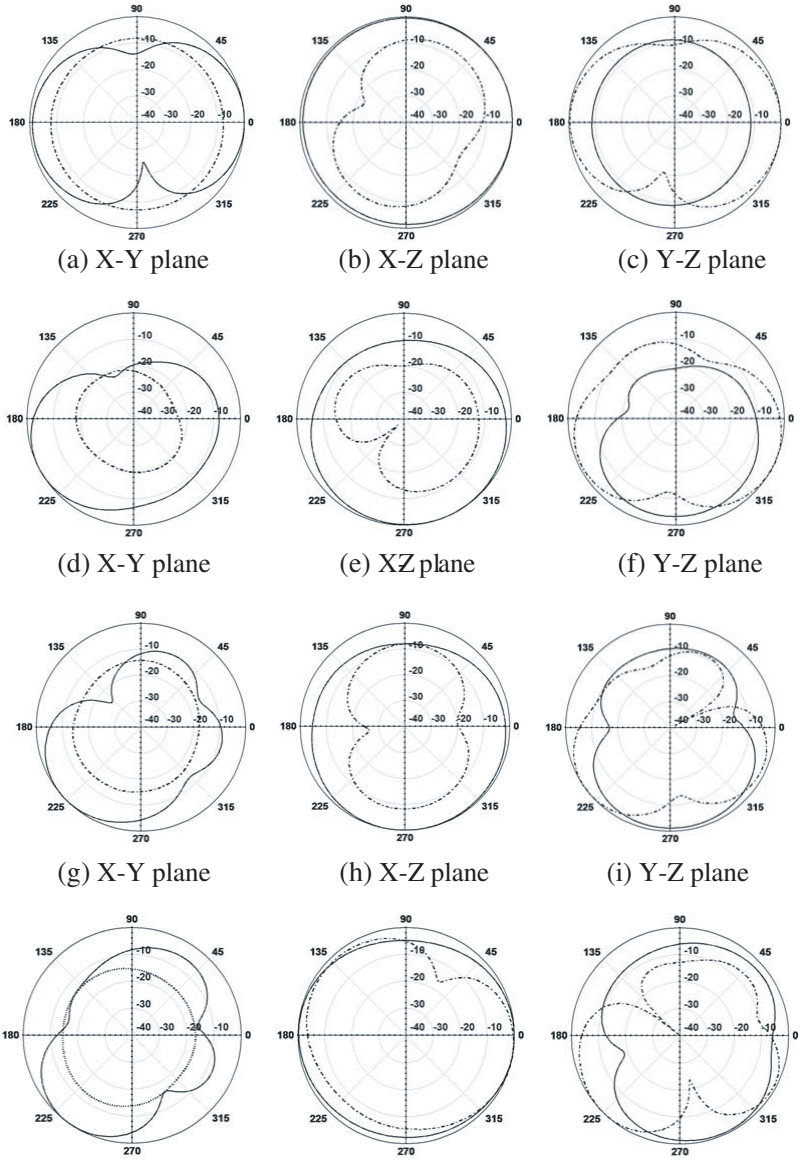

(a) X-Y plane (b) X-Z plane (c) Y-Z plane

(d) X-Y plane (e) XZ plane (f) Y-Z plane

(g) X-Y plane (h) X-Z plane (i) Y-Z plane

(j) X-Y plane (k) X-Z plane (l) Y-Z plane

Figure 13. Measured radiation pattern (a) $\sim$ (c) at 920 MHz, (d) $\sim$ (f) at 1.75 GHz, (g) $\sim$ (i) at 2.03 GHz, (j) $\sim$ (l) at 2.2 GHz. (E_φ: solid line, E_θ: dotted line).

include the GSM (880–960 MHz)/DCS (1710–1880 MHz)/PCS (1850–1990 MHz)/IMT-2000 (1920–2170 MHz), based on the results shown in Fig. 12.

4.2. Radiation Pattern and Gain

The measured far-field radiation patterns at different frequencies of the new quad-band antenna at 0.92, 1.75, 2.03, 2.2 GHz and in three orthogonal planes are depicted in Figs. 13(a)–(l), respectively. They are similar to those of other integrated antennas for mobile handsets. Referring to Fig. 13, the overall shape of the radiation patterns is suitable for mobile communications terminals. Figs. 14 and 15 show that the simulated and measured copolarized gains with GSM-900/DCS-1800/PCS-1900/IMT-2000 of the proposed antennas.

5. USER'S HAND EFFECTS ON ANTENNA PERFORMANCES

Effects of the user's hand on the proposed antenna were also studied. The experimental photo and simulated model are shown in Figs. 16(a) and 16(b), in which the parameter d indicates the distance from the top edge of the mobile phone to the top of user's thumb. From the simulated and measured S_{11} for cases with (d = 0, 20, 40, and 60 mm) and without user's hands are shown in Figs. 16(c) and 16(d), the measurement and simulation almost reaches an agreement. This agreement ensures reliable simulation results obtained from the simulation software SEM-CAD and the hand model whose relative

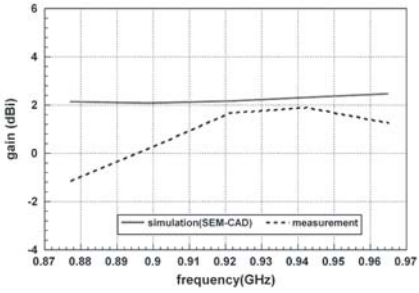

Figure 14. Simulated and measured co-polarized gain with GSM-900 of the proposed antenna.

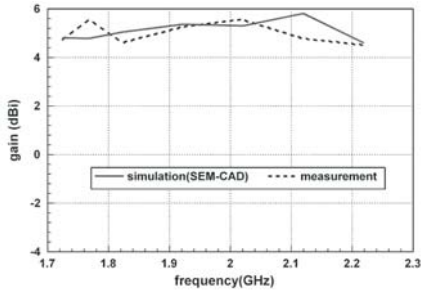

Figure 15. Simulated and measured co-polarized gain with DCS-1800/PCS-1900/IMT-2000 of the proposed antenna.

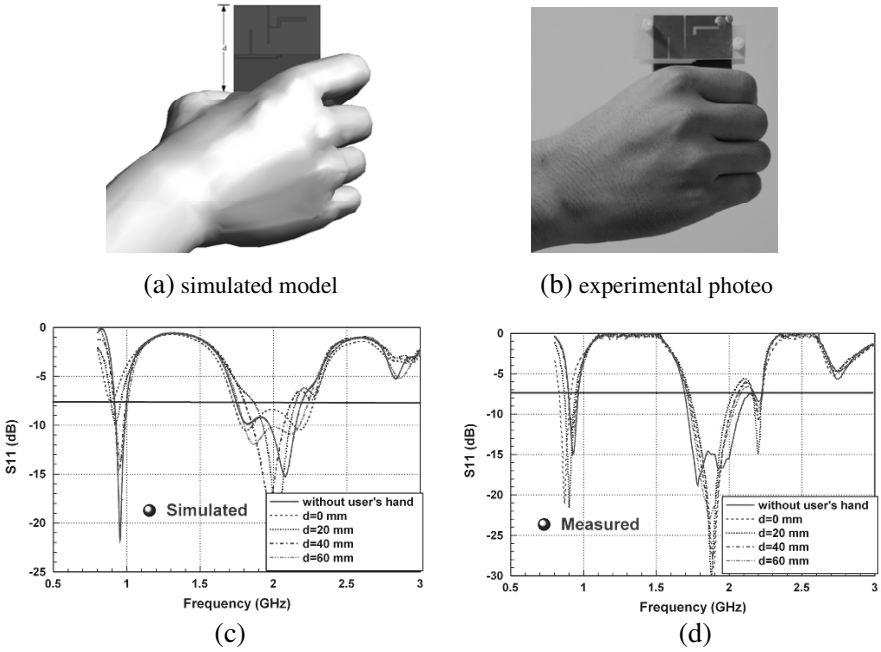

Figure 16. (a) Simulated model, (b) experimental photo, (c) simulated and (d) measured S_{11} for $d = 0$, 20, 40, and 60 mm for the proposed antenna with the user's hand.

permittivity and conductivity at the studied frequencies are obtained from [20]. Note that, in the experiment, the proposed antenna and the system ground plane are enclosed by a thin plastic housing to avoid direct contact with the user's hand, as shown in Fig. 3. Also, the relative permittivity of the plastic housing is chosen to be small or close to that of air so that the antenna performances are minimally affected by the presence of the plastic housing. From the results obtained, it is seen that the frequency detuning is larger for the case of $d = 0$ (the antenna is completely overlaid by the user's hand) than for the cases of $d = 20$, 40, and 60 mm.

Figure 17 shows the simulated radiation efficiency as a function of d. Note that there is geometry of the proposed antenna including plastic housing, as shown in Fig. 3. The proposed antenna and the system ground plane are enclosed by a thin plastic housing to avoid direct contact with the user's hand. The presence of the user's hand seems to result in a large decrease in the radiation efficiency. The efficiency decrease is also larger when d is smaller.

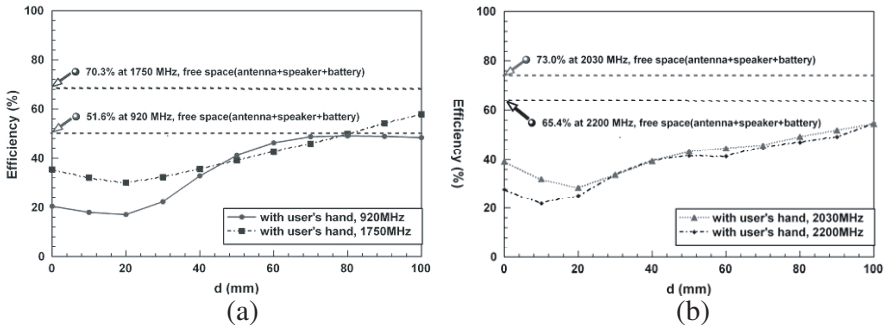

Figure 17. Simulated radiation efficiency as a function of d for the proposed antenna (a) 920 and 1750 MHz, (b) 2030 and 2200 MHz.

The simulated three-dimensional radiation efficiency obtained from SEM-CAD at 920, 1750, 2030 and 2200 MHz are also studied. It is observed that the radiation power is greatly absorbed by the user's hand in the forearm direction, leading to large distortions in the antenna radiation patterns. Much larger pattern distortions are seen when the distance d is smaller. The results indicate that the radiation patterns of the antenna are strongly dependent on the parameter d.

6. CONCLUSION

A small volume antenna of planar inverted F type with two open-ended parallel slots in the ground plane, locating almost under the primary radiating element, has been described and investigated. From the measured results, numerical simulations, and equivalent circuit model analysis, it has been found that by properly selecting dimensions of the slots, a significant improvement in the antenna operational bandwidth at the high frequency band can be achieved.

The presented bandwidth enhancement method allows for reducing the antenna volume without changing the geometrical shape of the primary radiating element. With its thin profile of 4 mm only, the proposed antenna is very promising for thin mobile phone applications. Furthermore, effects of the user's hand holding the studied mobile phone with the proposed antenna have been analyzed. Strong effects of the user's hand on the radiation efficiency and radiation pattern of the proposed antenna have been observed. When the user's hand is present, large decrease in the radiation efficiency is seen, which means the radiation power is absorbed by the user's hand. Large distortion in the antenna radiation patterns is also seen,

especially when the antenna is overlaid by the user's hand. The obtained results suggest that the effects of user's hand should be considered for mobile devices.

ACKNOWLEDGMENT

This research work was supported by the both National Science Council of the Republic of China under the Grant number NSC 98-2220-E-027-006 and NSC 98-2221-E-024-016.

REFERENCES

1. Tang, I-T., D.-B. Lin, W.-L. Chen, and J.-H. Horng, "Miniaturized hexaband meandered PIFA antenna using three meandered-shaped slits," *Microwave and Optical Technology Letters*, Vol. 50, No. 4, 1022–1025, Apr. 2008.
2. Chiu, C.-W., C.-H. Chang, and Y.-J. Chi, "Multiband folded loop antenna for smart phones," *Progress In Electromagnetics Research*, Vol. 102, 213–226, 2010.
3. Cabedo, A., J. Anguera, C. Picher, M. Ribo, and C. Puente, "Multi-band handset antenna combining PIFA, slots, and ground plane modes," *IEEE Transactions on Antennas and Propagation*, Vol. 57, No. 9, 2526–2533, Sep. 2009.
4. Chiu, C. W. and Y. J. Chi, "Planar hexa-band inverted-F antenna for mobile device applications," *IEEE Antenna and Wireless Propagation Letters*, Vol. 8, 1099–1102, 2009.
5. Picher, C., J. Anguera, A. Cabedo, C. Puente, and S. Kahng, "Multiband handset antenna using slots on the ground plane: Considerations to facilitate the integration of the feeding transmission line," *Progress In Electromagnetics Research C*, Vol. 7, 95–109, 2009.
6. Sun, J.-S. and S.-Y. Huang, "A small 3-D multi-band antenna of "F" shape for portable phones' applications," *Progress In Electromagnetics Research Letters*, Vol. 9, 183–192, 2009.
7. Saidatul N. A., A. A. H. Azremi, R. B. Ahmad, P. J. Soh, and F. Malek, "Multiband fractal planar inverted F Antenna (F-Pifa) for mobile phone application," *Progress In Electromagnetics Research B*, Vol. 14, 127–148, 2009.
8. Cheng P.-C., C.-Y.-D. Sim, and C.-H. Lee, "Multi-band internal monopole antenna for mobile handset applications," *Journal of Electromagnetic Waves and Applications*, Vol. 23, No. 13, 1733–1744, 2009.

9. Sun B. H., J. F. Li, and Q. Z. Liu, "Compact broad-band printed antenna for multi-functional mobile terminals," *Journal of Electromagnetic Waves and Applications*, Vol. 22, No. 8-9, 1292–1298, 2008.
10. Jensen, M. A. and Y. Rahmat-Samii, "EM interaction of handset antennas and a human in personal communications," *Proc. IEEE.*, Vol. 83, 7–17, Jan. 1995.
11. Rowell, C. and R. Murch, "A capacitively loaded PIFA for compact mobile telephone handsets," *IEEE Trans. Antennas Propagat.*, Vol. 45, 837–842, May 1997.
12. Taga, T., "Analysis of planar inverted-F antennas and antenna design for portable radio equipment," *Analysis, Design and Measurement of Small and Low-profile Antennas*, K. Hirasawa and M. Haneishi, Eds., Ch. 5, 161–180, Artech House, Norwood, MA, 1992.
13. Manteuffel, D., A. Bahr, D. Heberling, and I. Wolff, "Design considerations for integrated mobile phone antennas," *Proc. 11th Int. Conf. Antennas Propagat.*, Apr. 17–20, 252–256, 2001.
14. Vainikainen, P., J. Ollikainen, O. Kivekas, and I. Kelander, "Resonantor-based analysis of the combination of mobile handset antenna and chassis," *IEEE Trans. on Antennas Propagat.*, Vol. 50, No. 10, Oct. 2002.
15. Hossa, R., A. Byndas, and M. Bialkowski, "Improvement of compact terminal antenna performance by incorporating open-end slots in ground plane," *IEEE Microwave and Wireless Components Letters*, Vol. 14, No. 6, Jun. 2004.
16. Kabacik, P., R. Hossa, and A. Byndas, "Broadening the bandwidth in terminal antennas by tuning the coupling between the element and its ground," *IEEE Antennas and Propagation Society International Symposium*, Vol. 3A, 3–8, Jul. 2005.
17. Balanis, C. A., *Antenna Theory-analysis and Design*, 941, Wiley, New York, 1997.
18. Salonen, P., M. Keskilammi, and M. Kivikoski, "Single-feed dual planar inverted-F antennas with U-slot," *IEEE Trans. Antennas Propag.*, Vol. 48, No. 8, 1262–1264, Aug. 2000.
19. Nashhat, D., H. Elsadek, and H. Ghali, "Dual-Band reduced size PIFA antenna with U-slot for bluetooth and WLAN applications," *Proc. IEEE Antennas Propagation Int. Symp.*, 22–27, Columbus, OH, Jun. 2003.
20. SEMCAD, Schmid & Partner Engineering AG (SPEAG), Available: http://www.semcad.com.